




## ARTICLE OPEN ACCESS

# Kinetic Modeling of the Antibody Disulfide Bond Reduction Reaction With Integrated Prediction of the Drug Load Profile for Cysteine-Conjugated ADCs

Jan Tobias Weggen<sup>1</sup>  | Pedro González<sup>1</sup> | Kimberly Hui<sup>2</sup> | Ryan Bean<sup>2</sup> | Michaela Wendeler<sup>2</sup>  | Jürgen Hubbuch<sup>1</sup> 

<sup>1</sup>Institute of Process Engineering in Life Sciences, Section IV: Biomolecular Separation Engineering, Karlsruhe Institute of Technology (KIT), Karlsruhe, Baden-Württemberg, Germany | <sup>2</sup>Purification Process Sciences, Biopharmaceutical Development, BioPharmaceuticals R&D, AstraZeneca, Gaithersburg, Maryland, USA

**Correspondence:** Jürgen Hubbuch ([juergen.hubbuch@kit.edu](mailto:juergen.hubbuch@kit.edu))

**Received:** 5 July 2024 | **Revised:** 9 October 2024 | **Accepted:** 20 November 2024

**Keywords:** antibody-drug conjugate (ADC) | capillary gel electrophoresis (CGE) | cysteine conjugation | interchain disulfides | kinetic model | process development | reduction reaction

## ABSTRACT

Antibody-drug conjugates (ADC) constitute a groundbreaking advancement in the field of targeted therapy. In the widely utilized cysteine conjugation, the cytotoxic payload is attached to reduced interchain disulfides which involves a reduction of the native monoclonal antibody (mAb). This reaction needs to be thoroughly understood and controlled as it influences the critical quality attributes (CQAs) of the final ADC product, such as the drug-to-antibody ratio (DAR) and the drug load distribution (DLD). However, existing methodologies lack a mechanistic description of the relationship between process parameters and CQAs. In this context, kinetic modeling provides comprehensive reaction understanding, facilitating the model-based optimization of reduction reaction parameters and potentially reduces the experimental effort needed to develop a robust process. With this study, we introduce an integrated modeling framework consisting of a reduction kinetic model for the species formed during the mAb reduction reaction in combination with a regression model to quantify the number of conjugated drugs by DAR and DLD. The species formed during reduction will be measured by analytical capillary gel electrophoresis (CGE), and the DAR and DLD will be derived from reversed-phase (RP) chromatography. First, we present the development of a reduction kinetic model to describe the impact of reducing agent excess and reaction temperature on the kinetic, by careful investigation of different reaction networks and sets of kinetic rates. Second, we introduce a cross-analytical approach based on multiple linear regression (MLR), wherein CGE data is converted into the RP-derived DAR/DLD. By coupling this with the newly developed reduction kinetic model, an integrated model encompassing the two consecutive reaction steps, reduction and conjugation, is created to predict the final DAR/DLD from initial reduction reaction conditions. The integrated model is finally utilized for an *in silico* screening to analyze the effect of the reduction conditions, TCEP excess, temperature and reaction time, directly on the final ADC product.

## 1 | Introduction

Antibody-drug conjugates (ADCs) are a class of innovative therapeutics engineered to deliver potent cytotoxic drugs directly to cancer cells while minimizing damage to healthy

tissues (Chau, Steeg, and Figg 2019; Fu et al. 2022; Khongorzul et al. 2020). Consisting of monoclonal antibody (mAb), cytotoxic payload, and linker, ADCs offer precise targeting, enhancing efficacy and reducing systemic toxicity compared to traditional chemotherapy. ADCs constitute one of the fastest-

This is an open access article under the terms of the [Creative Commons Attribution-NonCommercial](https://creativecommons.org/licenses/by-nc/4.0/) License, which permits use, distribution and reproduction in any medium, provided the original work is properly cited and is not used for commercial purposes.

© 2024 The Author(s). *Biotechnology and Bioengineering* published by Wiley Periodicals LLC.

growing classes of anticancer drugs, with fourteen ADCs approved by the FDA as of 2023 and hundreds progressing in clinical trials (Metrangolo and Engelholm 2024). Driven by persistent research efforts in ADC design, such as more stable linkers, novel payloads and new conjugation strategies, the challenge to develop robust and scalable processes increases (Prashad et al. 2017; Sasso et al. 2023).

The potency of ADCs largely depends on the type of payload and the number of payload molecules attached, known as the drug-to-antibody ratio (DAR). Controlling the DAR and the drug load distribution (DLD) is crucial for optimizing the ADC therapeutic index, as every species within the DLD exhibits distinct pharmacokinetics and efficacy (Behrens and Liu 2014; Kamath and Iyer 2015). A central consideration in this context is the conjugation strategy, which facilitates the connection of the mAb and linker-payload (Gordon et al. 2015). Payload conjugation to cysteine residues that are engaged in the four native interchain disulfide bonds is a common conjugation strategy. While this approach is widely used, it can minimally alter the mAb structure and negatively impacts stability, particularly for higher DAR species (Adem et al. 2014; Guo et al. 2016). With regard to the conjugation process, this approach involves a two-step reaction workflow: an initial mild reduction of the disulfide bonds of the mAb, followed by conjugation of the cytotoxic payload to the reactive cysteine residues. The final DAR for cysteine-linked ADCs ranges from 2 to 8. The reduction reaction is the key step for determining the DAR, as it generates a specific number of binding sites for the payload (Metrangolo and Engelholm 2024; You et al. 2021). The reaction's outcome, including the formation of positional isomers, depends on the choice of reducing agents and various process parameters such as reducing agent concentration, reaction time, temperature and pH (Matsuda and Mendelsohn 2021; Sun et al. 2005). However, comprehensive understanding of the cysteine-based reaction process is limited (Matsuda et al. 2020; Nadkarni et al. 2018; Song et al. 2022). An additional research focus is on improving DAR homogeneity by cross-linking payloads (Behrens et al. 2015) or addition of metal ions (You et al. 2021).

Initiated by the FDA (ICH 2008), the concept of quality by design (QbD) promotes the utilization of modeling techniques to deepen process understanding of unit operations, forecast product behavior, and optimize processes. Consequently, process models have recently gained popularity for a variety of purposes for biopharmaceuticals and allow process developers to identify optimal reaction conditions based on fundamental knowledge of the reaction mechanisms during manufacturing (Narayanan et al. 2020; Smiatek, Jung, and Bluhmki 2020). To model biochemical reactions, kinetic studies are usually performed to gain knowledge about complex biochemical reaction mechanisms (Taylor et al. 2022). To construct mathematical process models for these reactions, the most challenging aspects are simultaneously identifying the reaction stoichiometry, inferring the structure of the reaction network, and estimating model parameters (Chou and Voit 2009). Various solutions have been proposed in the literature to address these challenges, for example, S-systems (Forster et al. 2023), target factor analysis (Fromer, Georgakis, and Mustakis 2023), automated reaction network generation and identification

(Taylor et al. 2021), and chemical reaction neural networks (Ji and Deng 2021).

With regard to modeling of the ADC conjugation process, recent studies focused on the conjugation kinetic (Andris, Seidel, and Hubbuch 2019) for site-specific ADCs, or the reduction reaction for cysteine-conjugated ADCs (Nayak and Richter 2023). The latter provides quantitative insights into the reduction mechanisms of interchain disulfide bonds and the use of the kinetic model for process optimization, relying on a complex mathematical approach to resolve positional isomers by hydrophobic interaction chromatography (HIC) and reversed-phase ultrahigh-performance liquid chromatography (RP-UHPLC).

In this study, we introduce the combination of reduction kinetic model and linear regression to model the reduction reaction with directly determining the DAR/DLD at the conjugation endpoint. For the development of these models, we performed reduction kinetic studies with varying initial conditions, namely the mAb concentration, reducing agent concentrations, as well as the reaction temperatures, while the subsequent conjugation reactions were conducted under the same reaction conditions. Samples were analyzed by both non-reducing capillary gel electrophoresis-sodium dodecyl sulfate (CGE-SDS, or herein shortly CGE) to quantify the reduced species, and RP-UHPLC to determine the DAR/DLD. Based on species formed during reduction, a mechanistic kinetic model for the interchain disulfide bond reduction reaction is developed, providing insights into the complex reduction mechanism. Here, various chemical reaction networks (CRNs) with different sets of kinetic rates are proposed and the most suitable CRN was selected. Then, multiple linear regression (MLR) models are employed to predict the final DAR and the percentages of the drug load distribution (DLD-%) from the species formed during the reduction reaction. Finally, the reduction kinetic model and the MLR models are combined, creating an integrated modeling tool enabling *in silico* screening of process parameters in the cysteine-based reaction workflow.

## 2 | Material and Methods

### 2.1 | Experiments

The experiments involved two sequential reaction steps: reduction and conjugation. The reduction conditions were varied to investigate their influence on the partial reduction kinetics of the interchain disulfide bonds. Tris(2-carboxyethyl) phosphine hydrochloride (TCEP) was used as reducing agent, as this reduces both the two disulfide bonds between the two heavy chains (inter HH) and the bonds between each heavy and light chain (inter HL). The reduction of intrachain disulfides was excluded, given that they are known to remain intact under TCEP treatment (You et al. 2021). In the subsequent conjugation reaction, maleimide-functionalized payload is conjugated to these reduced disulfide bonds under constant reaction conditions. Non-reducing CGE was used to track the kinetics of the intact mAb and the generated fragments (L (light chain), H (heavy chain), HL, HH, HHL) over time, which are generated as

disulfide bonds are reduced. This provided a quantitative measurement of the reduction kinetics. Two IgG1 mAbs, which will be referred to as mAb1 and mAb2, were employed in the scope of the experiments.

### 2.1.1 | Chemicals and Buffers

The chemicals used in this study were obtained from EMD Millipore, unless otherwise stated. Standard conjugation buffer was 20 mM NaH<sub>2</sub>PO<sub>4</sub> (J.T. Baker), 1 mM EDTA in ultrapure water at pH of 7.0. TCEP-HCl (VWR) was used to reduce the mAb. For conjugation, a maleimide-functionalized payload (proprietary topoisomerase inhibitor, molecular weight of approx. 1200 Da) was dissolved in dimethyl sulfoxide (DMSO, Sigma-Aldrich). For sample treatment for DAR analysis, samples were diluted in denaturing buffer containing guanidine HCl (Thermo Scientific), Tris (Thermo Scientific), EDTA and dithiothreitol (Thermo Scientific) at pH 7.6. RP-UHPLC was performed using acetonitrile (VWR) and HPLC water (VWR), both with 0.1% (v/v) trifluoroacetic acid (Thermo Scientific). For sample treatment for CGE analysis, samples were diluted in 1 M Tris, pH 7.0.

### 2.1.2 | Reduction Kinetic Procedure

Initially, the mAb was thawed and diluted to the desired starting mAb concentration in conjugation buffer. A 50 mM TCEP solution was prepared in conjugation buffer and pH adjusted to 7 using NaOH (J.T. Baker). The reduction reaction was started by adding a predetermined volume of the 50 mM TCEP solution to the diluted mAb to reach a desired molar excess of TCEP over mAb. The reaction was allowed to shake on an orbital shaker (Eppendorf) at the specified temperature. Seven kinetic samples were taken at 5, 10, 20, 30, 60, 120, and 240 min. The reduction reaction was quenched by addition of a 12-fold molar excess of payload (25 mM solution in DMSO) to conjugate all available cysteines, thus preventing reduced disulfides from reforming. DMSO was spiked into the conjugation reaction to reach 10% (v/v) DMSO to improve payload solubility during conjugation. The conjugation reaction was allowed to proceed on a tube rotator at room temperature for 30 min. In 17 runs using mAb1, the reduction temperature, the initial mAb concentration, and the TCEP excess were varied ( $n = 119$  samples). Three additional runs with mAb2 were performed ( $n = 21$  samples). The reduction reaction conditions are summarized in Table 1. Since each experimental condition was performed only once, the potential variability of the experimental procedure was assessed independently, indicating good robustness (see Supporting Information).

### 2.1.3 | Sample Analytics

#### 2.1.3.1 | Non-Reducing Capillary Gel Electrophoresis.

To quantify the partial reduction of the mAb, samples were analyzed with non-reducing CGE-SDS on a PA800+ capillary electrophoresis instrument (AB Sciex) using the assay protocol as published in Cao et al. (2019). Samples were

electrokinetically injected into the capillary and separated in reverse polarity. Each sample was analyzed once, as the CGE method demonstrated robustness with a relative standard deviation (RSD) ranging from 1% to 3% (data not shown). The resulting exported data contained the fractions, denoted as  $p_i$ , of intact mAb monomer and its reduced fragments within the reaction mixture. The molar concentrations of each species  $\tilde{c}_i$  was converted using the respective mAb concentration of the sample  $c_{\text{mAb}}$  and the molar mass of the respective species  $\tilde{M}_i$  according to

$$\tilde{c}_i = p_i \cdot \frac{c_{\text{mAb}}}{\tilde{M}_i} \quad (1)$$

#### 2.1.3.2 | Reducing Reversed-Phase Ultra-High Performance Liquid Chromatography.

To determine the DAR and the DLD, each sample was analyzed using RP-UHPLC. Details about sample treatment procedure and the analytical workflow can be found in Cao et al. (2019). The data for each sample contained the peak areas  $A$  of un- and mono-conjugated light chain, L0 and L1, and of un-, mono-, bi- and tri-conjugated heavy chain, H0, H1, H2 and H3, respectively. The percentages of the two light chain species and four heavy chain species were calculated by dividing the peak area through the total peak area of all light chain species,  $A_{L,\text{tot}}$ , or heavy chain species,  $A_{H,\text{tot}}$ . The DLD of each sample thus consisted of the percentages of all six species [%L0 %L1 %H0 %H1 %H2 %H3]. The respective DAR was calculated according to

$$\text{DAR} = 2 \left( \frac{A_{L1}}{A_{L,\text{tot}}} + \frac{A_{H1} + 2A_{H2} + 3A_{H3}}{A_{H,\text{tot}}} \right) \quad (2)$$

The raw data from both analytics are provided as Supporting Information S2.

## 2.2 | Data Organization

In this study, two model types were developed and the data were organized differently: (1) For development of the reduction kinetic model, the full reduction kinetic data set from CGE for mAb1 was manually split based on the reduction temperature into a training subset (4°C, 20°C and 37°C) with 15 runs and an independent test subset (12°C) with two runs. The training subset was used for model development and selection, and the test set for independent validation of the reduction kinetic model. The mAb2 CGE data set was excluded from the reduction modeling process, as the two mAbs exhibited differences in their reduction behavior. (2) For the development of the MLR models the full data set comprising both CGE (119 time samples as rows, 6 CGE species as columns) and RP-UHPLC (119 time samples as rows, DAR + 6 DLD-% as columns) for mAb1 was used. The data set for mAb2 was then applied for external evaluation.

## 2.3 | Mechanistic Reduction Kinetic Modeling

The reduction of the interchain disulfide bonds by TCEP results in the occurrence of reduced fragments, HHL, HH, and HL, and

**TABLE 1** | List of conducted reduction experiments using different mAbs, reduction reaction temperatures, initial mAb concentration and initial TCEP excess. Additionally, the corresponding subset for each run is given.

RunID	mAb	Temperature (°C)	$c_{\text{mAb}}$ (g/L)	Molar TCEP excess/-	Subset
1	mAb1	20	15	2	Training
2	mAb1	20	15	3	Training
3	mAb1	20	15	4	Training
4	mAb1	20	15	6	Training
5	mAb1	20	15	8	Training
6	mAb1	20	3.75	4	Training
7	mAb1	20	7.5	4	Training
8	mAb1	20	10	4	Training
9	mAb1	37	15	2	Training
10	mAb1	37	15	4	Training
11	mAb1	37	15	6	Training
12	mAb1	37	15	8	Training
13	mAb1	4	15	2	Training
14	mAb1	4	15	4	Training
15	mAb1	4	15	8	Training
16	mAb1	12	15	4	Test
17	mAb1	12	15	6	Test
18	mAb2	20	15	4	External
19	mAb2	20	20	8	External
20	mAb2	20	20	10	External

single chains, L and H, as measured by CGE. To understand the reaction, mechanistic modeling was chosen over statistical modeling for its ability to capture the underlying reaction mechanisms, unlike statistical models that rely solely on data correlations. Based on kinetic rate laws, mechanistic models allow for extrapolation outside the experimental data, whereas statistical models are limited to predictions within the range of their training data. This reduces experimental workload and accelerates process development by enabling the efficient screening of process conditions such as mAb concentration, TCEP excess, and reduction time. The development of the mechanistic reduction kinetic model involved the iterative selection of a suitable CRN and a set of kinetic rates accounting for the temperature-dependency of the reaction via the Arrhenius approach. For the first task, different CRNs were proposed and evaluated using the same assumption for kinetic rate discrimination. After selecting the most suitable CRN, the set of kinetic rates was further investigated in more detail to improve model performance.

### 2.3.1 | Chemical Reaction Network Construction and Kinetic Rate Discrimination

For the construction of the CRN, special focus was on the two inter HH disulfide bonds localized in the IgG hinge region. As the CGE is unable to differentiate between fragments with two or one intact inter HH disulfide bonds, it was not possible to determine whether

the reduction of these bonds occurred stepwise. To assess the impact of the reduced form of these intermediate on the reaction kinetics, two CRN types were constructed: In the *NoInt* CRN, the reduction of the two hinge bonds is considered as single reaction step yielding seven reaction species (= seven CGE species) and six reactions. Conversely, in the *WithInt* CRN, a two-step reduction in the hinge region is included to account for the three non-observable intermediates, IntactR, HHLR and HHR (R = reduced form), resulting in a more complex CRN with ten species and eleven reactions. Additionally, a reforming of the reduced species was observed in the data, which coincides with a decreasing DAR value. Therefore, a reoxidation of the reduced disulfide bonds was assumed in the model assigning a backwards reoxidation reaction for each forward reduction step, leading to two additional variants of each CRN type, *WithInt + ReOx* (graphically summarized in Figure 1A) and *NoInt + ReOx* (given in the Supporting Information). To parametrize these CRNs, kinetic rates needed to be assigned to each individual reaction step. As suggested by Chen et al. (2024) that TCEP reduction kinetically favors the inter HL over the inter HH bonds, all individual rates belonging to either inter HH or inter HL reduction/reoxidation were lumped. As HH reoxidation rates were observed to be substantially slower in comparison to the other kinetic rates, the respective reaction steps were removed in all CRNs that account for the reoxidation. Consequently, this resulted in the simple models with two (for CRNs without ReOx) or three kinetic distinct kinetic rates (for CRNs with ReOx, “3k-model”), which were used as baseline rate discrimination to independently analyze the CRN performance.

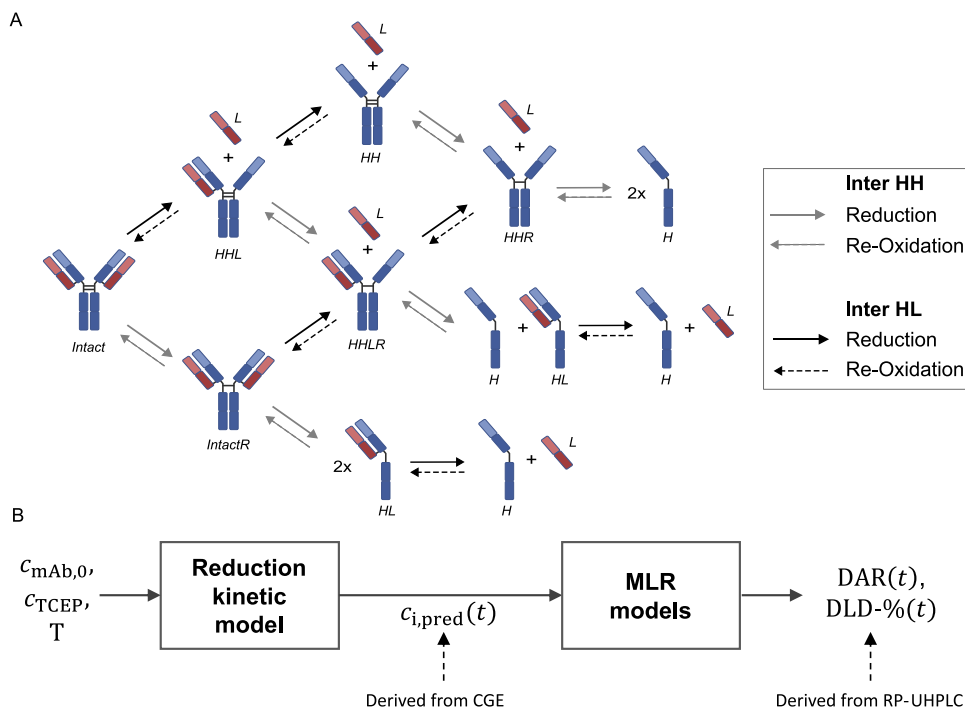


**FIGURE 1** | (A) Proposed structure of a CRN with intermediates and reoxidation reaction. Black and gray arrows indicate reactions between inter heavy-heavy (HH) or inter heavy-light (HL) chains. Heavy chains are colored in blue and light chain are colored in red. (B) Schematic representation of the integrated modeling architecture for the sequential combination of the newly developed reduction kinetic modeling with the MLR models predicting the DAR and DLD percentages (DLD-%).

Additionally, two other sets of kinetic rates with more advanced kinetic rate discriminations were evaluated. A second, refined model was defined that specifically discriminates the reduction/reoxidation belonging to each CGE-observed fragment (e.g. three different rates for the three inter HL reduction of Intact, HHL and HL). Based on the 3k-model, this assumption tripled the number of rates resulting in nine kinetic rates (“9k-model”). Nayak and Richter (2023) presented a reduction kinetic model, that indicated a considerable difference between the first and second reduction steps for the inter HH reduction. This finding motivated the design of a third discrimination, which uses a similar approach as the 9k-model, but instead only distinguishes the stepwise inter HH reduction step with two rates, leading in total to eight kinetic rates (“8k-model”). Table 2 summarizes the investigated reduction models. A list of the reactions and the corresponding rates is given in Supporting Information.

### 2.3.2 | Temperature Modeling

The Arrhenius equation was applied to model the temperature effect of the kinetic rates. This led to double the amount of necessary model parameters in each model, as each rate was split into two Arrhenius parameters. To avoid optimization problems due to high correlation between the Arrhenius parameters, activation energy,  $E_a$ , and pre-exponential factor,  $k_0$ , it is common to use a reparametrized expression of the Arrhenius equation (Schwaab and Pinto 2007). The herein used expression is

$$k(T) = k_{T_{ref}} e^{-\frac{E_a}{R} \left( \frac{1}{T} - \frac{1}{T_{ref}} \right)}, \quad (3)$$

where  $R$  denotes the ideal gas constant,  $T_{ref}$  is the reference temperature and  $k_{T_{ref}}$  presents the kinetic rate at the reference temperature.  $T_{ref} = 293.15$  K was chosen adequately to minimize the parameter correlation.

### 2.3.3 | Parameter Estimation

All tested models were implemented as ordinary differential equations (ODE) in MATLAB (The MathWorks Inc.) and numerically solved using the *ode15s* solver. The kinetic rates were estimated based on the nonlinear least squares approach. A custom loss function was utilized that computed the error between the CGE-derived experimental and the model-predicted concentrations. In case of the models with intermediates, the concentrations of the reduced intermediates and the respective non-reduced intermediates were summed up to align with the CGE-derived molar concentrations of the species. To ensure an equal weighting of the six reaction species, the species errors were normalized to the maximum species concentration within the full data set. A constant variance for all data points is assumed, as the CGE measurement error was found to be uniform across all species. As initial parameter values, all  $E_a$  were set to 20 kJ/mol, and all  $k_{T_{ref}}$  to  $1 \times 10^{-4}$  L( $\mu$ mol s) $^{-1}$ . The model parameters were optimized using *lsqnonlin*. The uncertainty of the estimated parameters was assessed via 95% confidence intervals (CI) computed using *nlparci*.

**TABLE 2** | Summary of the tested CRNs and parameter assignments.

No	Intermediates (Int)	Reoxidation (Re-Ox)	Rates (k)	Rate discrimination
1	No	No	2	Groups inter HL/HH reduction
2	No	Yes	3	Groups inter HL and HH reduction/reoxidation
3	Yes	Yes	3	Groups inter HL and HH reduction/reoxidation
4	Yes	Yes	9	Individual rates for each fragment
5	Yes	Yes	8	Same as 9k, but for inter HH two rates for the stepwise reduction

### 2.3.4 | Model Error, Selection and Validation

The resulting model performance was quantified by the normalized root mean square error (nRMSE) for each run and for each species computed as

$$\text{nRMSE}_i = \frac{\sqrt{\frac{1}{N} \sum_{i=1}^N (c_i - \hat{c}_i)^2}}{\bar{c}_i}, \quad (4)$$

where  $N$  is the number of samples, and  $c_i$ ,  $\hat{c}_i$  and  $\bar{c}_i$  denote the measured, model predicted, and mean measured concentration of the  $i$ th species, respectively. For model selection, the prediction error of the model was assessed based on both cross-validation of the 15 training runs (nRMSE<sub>CV</sub>) and on the two test runs (nRMSE<sub>P</sub>). A leave-one-run-out scheme was used for the cross-validation, wherein each run was systematically excluded one time and the resulting nRMSE<sub>CV</sub> values for all rotations were averaged. Additionally, the corrected Akaike's information criterion (AICc) was employed as a balanced measure between the goodness of fit and the model complexity. The AICc is calculated using

$$\text{AICc} = N \cdot \ln\left(\frac{\text{SSE}}{N}\right) + 2\delta + \frac{2\delta(\delta+1)}{N-\delta-2} + N \cdot \ln(2\pi) + N, \quad (5)$$

where SSE is the sum of squared error between measured and predicted concentration and  $\delta$  represents the number of model parameters.

## 2.4 | Integrated Reduction Kinetic Modeling

As the reduction reaction is the governing step due to its higher reaction time compared to the conjugation reaction (Nayak and Richter 2023), a subsequent model was incorporated to directly estimate the final DAR and the DLD-% from each state in the reduction kinetic without explicit consideration of the conjugation kinetic. This sequential combination with the newly developed mechanistic reduction kinetic model allowed then to perform an integrated kinetic modeling of the DAR and the DLD-% with regard to the initial reduction reaction conditions, that is,  $c_{\text{mAb},0}$ , TCEP excess, and the temperature. A schematic illustration of this model framework is shown in Figure 1B.

### 2.4.1 | Final DAR and DLD-% Estimation From CGE or Reduction Model Prediction

Multiple linear regression (MLR) models were employed to establish cross-analytical, functional mappings from the reduction state to the final conjugation outcome at each time point. The choice of a linear model was motivated by the robust linear correlation observed between the two analytical data sets (see Supporting Information S1: Figure S4). For one sample, the regression problem can be formulated as shown in Equation (6), where the concentrations of the six reduction species ( $c_{\text{intact}}$ ,  $c_{\text{HHL}}$ ,  $c_{\text{HH}}$ ,  $c_{\text{HL}}$ ,  $c_{\text{H}}$ ,  $c_{\text{L}}$ ) serve as the independent variables to predict the dependent variable,  $y$ , being either the RP-derived DAR or one of the six DLD-% (L0, L1, H0, H1, H2, and H3):

$$y = \beta_0 + \beta_1 c_{\text{intact}} + \beta_2 c_{\text{HHL}} + \beta_3 c_{\text{HH}} + \beta_4 c_{\text{HL}} + \beta_5 c_{\text{H}} + \beta_6 c_{\text{L}} + \epsilon, \quad (6)$$

where  $\beta_n$  represents the regression coefficients and  $\epsilon$  the error term. To fit the regression coefficients, the independent variables were structured as matrix with the six reduction species as columns and the time samples stacked as rows, while the different dependent variables were represented as arrays, each containing single values corresponding to each time sample. To ensure uniform consideration of the entire concentration range, the input concentrations were normalized by the respective mAb concentration. The function *fitlm* in Matlab was used for calibrating the MLR models. In a first step, this approach was evaluated utilizing the experimental CGE data as model input. Here, the mAb1 data set was randomly split into training and test set with a ratio of 75%/25%. Training and test error between the MLR-predicted and experimental DAR/DLD-% were quantified by the  $R^2$ . Subsequently, the MLR models were independently tested on the external data set of mAb2 to evaluate the potential generalizability of this approach. In a second step, the kinetic model predictions of the newly developed at each experimental time point were employed as model input. A recalibration of the MLR models was required due to the differences between experimental CGE and model-predicted reduction concentrations. For consistency, the same random training and test split was used in both instances. It is worth noting that this approach is applicable only when a sufficiently high payload excess is utilized to conjugate all reduced disulfide bonds.

## 2.4.2 | Integrated In Silico Screening and Process Optimization

To demonstrate the utility of the developed integrated framework in assisting ADC process development, an in silico screening of the reduction reaction conditions was performed. Two case scenarios were considered, wherein two out of the four possible process parameters (temperature, TCEP excess, mAb concentration and reduction time) were varied: In the first scenario, both reduction temperature and TCEP excess were varied within intervals of [4, 37]°C and [2, 8], respectively, while the reduction time was fixed to 120 min. In the second scenario, both reaction time and TCEP excess were varied within intervals of [0, 240] in and [2, 8], respectively, with the temperature set at 20°C. The initial mAb concentration was set to 15 g/L for both scenarios. Utilizing the calibrated reduction kinetic model, the resulting reduction species concentrations were systematically screened for varying initial conditions. These concentrations were then used to predict the DAR and DLD-% using the previously calibrated MLR models.

In the last part, a theoretical study was conducted to highlight the usability of the framework for identifying the appropriate reaction conditions for an exemplary target DAR of 3. Since reducing the amount of high-loaded species is often a requirement (Prashad et al. 2017), an additional objective was included to ensure that the percentage of H<sub>2</sub> remained below 12%. Similar to the in silico screening, individual DAR kinetics were simulated under varying temperature and TCEP excess to estimate the optimal reaction times for achieving the desired DAR.

## 3 | Results and Discussion

### 3.1 | Kinetic Modeling of Interchain Disulfide Bond Reduction Reaction

#### 3.1.1 | Model Development: Selection of CRN and Parameter Set

Five candidate reduction models were evaluated by their model error. Figure 2 illustrates the cross-validation and test nRMSE values, respectively, for each model with regard to the individual reduction species, along with the average nRMSE. The first three models represent different CRN variants under the same kinetic rate assumption. When comparing the first two models, the addition of the reoxidation reactions consistently improves the prediction of each species all species, except for H, resulting in an average nRMSE reduction of 24% and 22% for the CV and the test set, respectively. A particularly strong reduction was found for the intermediates HH and HL as well as for the species L. It is known that reoxidation can be provoked by the presence of dissolved oxygen (Hutterer et al. 2013; Wang et al. 2015). While Tang et al. (2020) found that the oxidation of reduced inter HH disulfide bonds tends to be generally more pronounced compared to inter HL, our results instead indicated that inter HH reoxidation is negligible. This discrepancy suggests either a structural difference among the studied mAbs affecting the reactivity of certain cysteines or other mechanisms, such as preferred de-conjugation of drug molecules bound in the inter HL region, that cause the

reforming of these bonds and herein being considered as reoxidation.

A further consistent improvement, except for the prediction of intact mAb, was achieved when including the intermediates with an average nRMSE reduction of 16% and 8% compared to the *NoInt + ReOx* model. The consideration of the reduced intermediates agrees with the structure of the aforementioned reduction kinetic model by Nayak and Richter (2023). Although these intermediates are not directly distinguishable by the CGE method, their consideration in the CRN contributes to improving the model, particularly concerning the intermediates HH and HL, which can be attributed to higher model flexibility due to the increased number of possible reactions.

Therefore, the *WithInt + ReOx* CRN was subsequently chosen for further model finetuning using two additional kinetic rate discriminations, 8k- and 9k-model. In comparison to the *WithInt + ReOx* with three ks, both sets of kinetic rates demonstrated similar error reductions of approximately 27% and 40% for cross-validation and test set, respectively. It was observed that this improvement primarily originates from an enhanced prediction accuracy for Intact, HHL and HH. The lowest AICc value was achieved for the 8k-model with 24.96 in comparison to the 9k-model with 35.84 suggesting a reasonable accurate model fit while minimizing the model complexity. The final use of the 8k-model for the further modeling purpose was justified by its lowest AICc value.

#### 3.1.2 | Mechanistic Insights

Insights into the kinetic mechanisms can be derived from the estimated kinetic rates. Figure 3 displays the estimated rates  $k_{i,20^{\circ}\text{C}}$  for the 8k-model (estimated  $E_A$  values are given in Supporting Information). The kinetic rates are grouped according to the three superordinated reaction steps. The three rates associated with the inter HL disulfide reduction for the three species, Intact (including IntactR), HHL (including HHLR), and HL, showed a decreasing trend from  $6.98 \times 10^{-4}$  to  $6.81 \times 10^{-5} \text{ L} (\mu\text{mol s})^{-1}$ . These differences might be explained by the different amount of available disulfide bonds (two in case of Intact, one for HHL and HL) and that each reduced disulfide bond might affect the conformational structure of the antibody resulting in a different susceptibility for TCEP reduction. Furthermore, it can be observed that the first inter HL reduction is faster compared to the first inter HH reduction. This is in agreement with Chen et al. (2024) who found that the inter HL reduction is kinetically favored over the HH reduction. A reason for this could be the higher solvent accessible surface area, as demonstrated with MD simulations (Song et al. 2022). With regard to the inter HH reduction, the kinetic rate of the second disulfide reduction,  $k_5$ , increases 18-fold compared to the first disulfide reduction  $k_4$ . This agrees with findings by both Liu et al. (2010), who suggest a conformational change in the hinge region once one inter HH bond is reduced resulting in greater exposure, and Nayak and Richter (2023), who hypothesize a “zipper”-like effect due to the increased flexibility in the CH<sub>2</sub> domain.

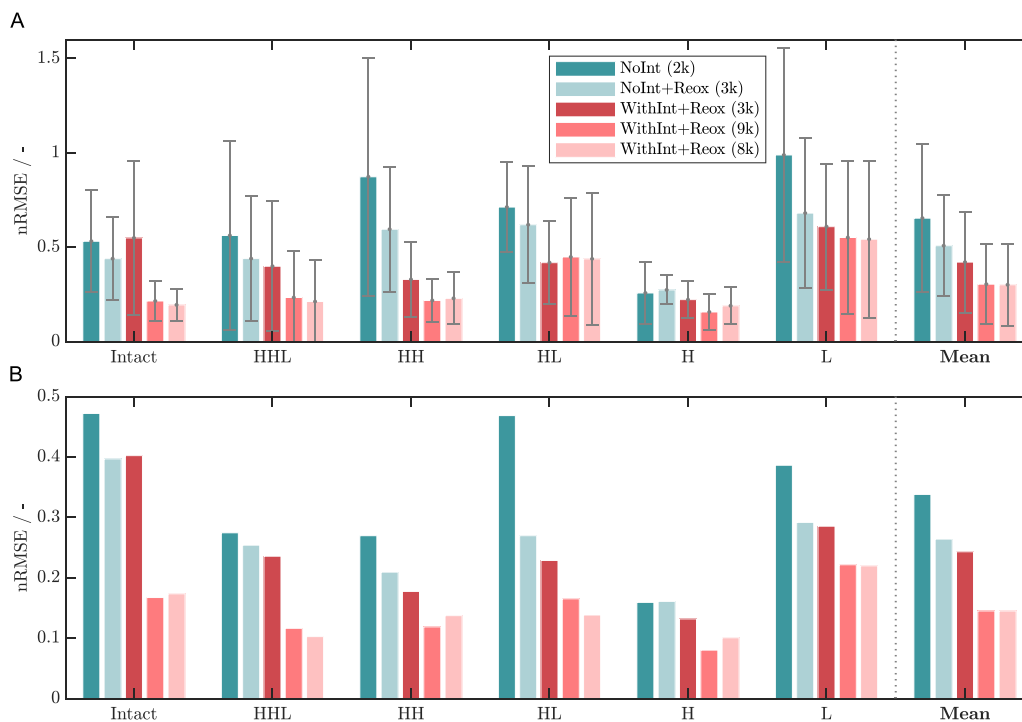


**FIGURE 2** | Comparison of the five evaluated reduction models with regard to the species-resolved and the mean nRMSE for the cross-validation (A) and the test runs (B). For the cross-validation, the bar represents the average nRMSE and the error bars indicate the standard deviation over all CV rotations.

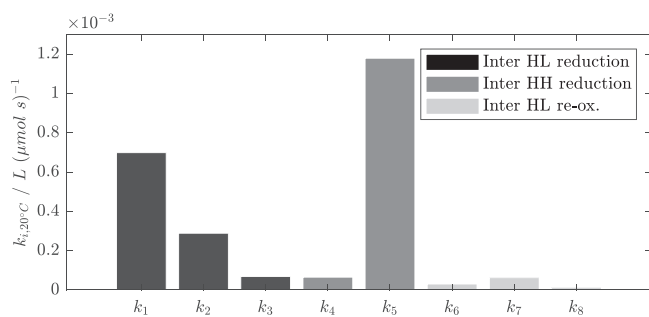


**FIGURE 3** | Estimated kinetic rates at the reference temperature of 20°C for the 8k-model.

An observation of the CIs of the estimated parameters (given in Supporting Information S1: Table S4), showed that CIs for most of the parameters range between 25% and 60% which indicates an acceptable parameter quality (Sin and Germaey 2016). Considerable wider CIs, especially for the  $E_a$  parameters associated with the reoxidation reactions, were observed suggesting that the data is not informative enough to precisely estimate these parameters. This could have multiple root causes such as the consideration of non-observable intermediates or the analytical error of the CGE method, which tends to increase for lower concentrations (Sänger-van de Griend 2019). The CIs of the  $E_a$  parameters are expected to decrease when more temperatures are added.

### 3.1.3 | Kinetic Model Predictions

A major advantage of a kinetic model is the ability to describe the reacting species' time-course for varying process parameters.

To thoroughly assess the model's performance on each run, the experimental versus predicted kinetics (cross-validation) using the 8k-model are plotted in Figure 4A. According to the CGE data, an increasing TCEP excess generally led to faster generation and higher ratios of H and L in the reduction reaction, while an increase in temperature caused faster kinetics and more pronounced reoxidation reactions. This dynamic occurred mainly for the species L at lower TCEP excesses. Interestingly, the species HH is generated at higher concentrations with decreasing temperatures, while at the same time the species HL appears to be inversely affected by the temperature. This contradictory influence of the temperature reflects the impact of the varying temperature-dependencies on the individual reaction pathways. A similar behavior for HH/HL was observed in a related process characterization study (Nadkarni et al. 2018).

In general, the model represents the observed trends in the CGE data accurately. To better illustrate the model error concerning temperature, TCEP excess, and species, the resulting species nRMSE for each cross-validated run is depicted in Figure 4B. The model demonstrates higher accuracy at the 4°C and 20°C kinetics, particularly at low TCEP excess and low mAb concentration. In contrast, the model accuracy decreases for the reduction at 37°C and at high TCEP excess, particularly for the species HL and L, as indicated by their higher nRMSE values at 20°C and 37°C. This corresponds to the larger error bars for these species in the cross-validation (cf. Figure 2). Overall, certain species, namely, H, HHL, and Intact are more precisely captured by the model. The decreased performance on the 37°C kinetics might be caused by non-parametrized effects increasingly occurring at higher temperatures, such as de-conjugation (Chen et al. 2016) or side reactions between TCEP and



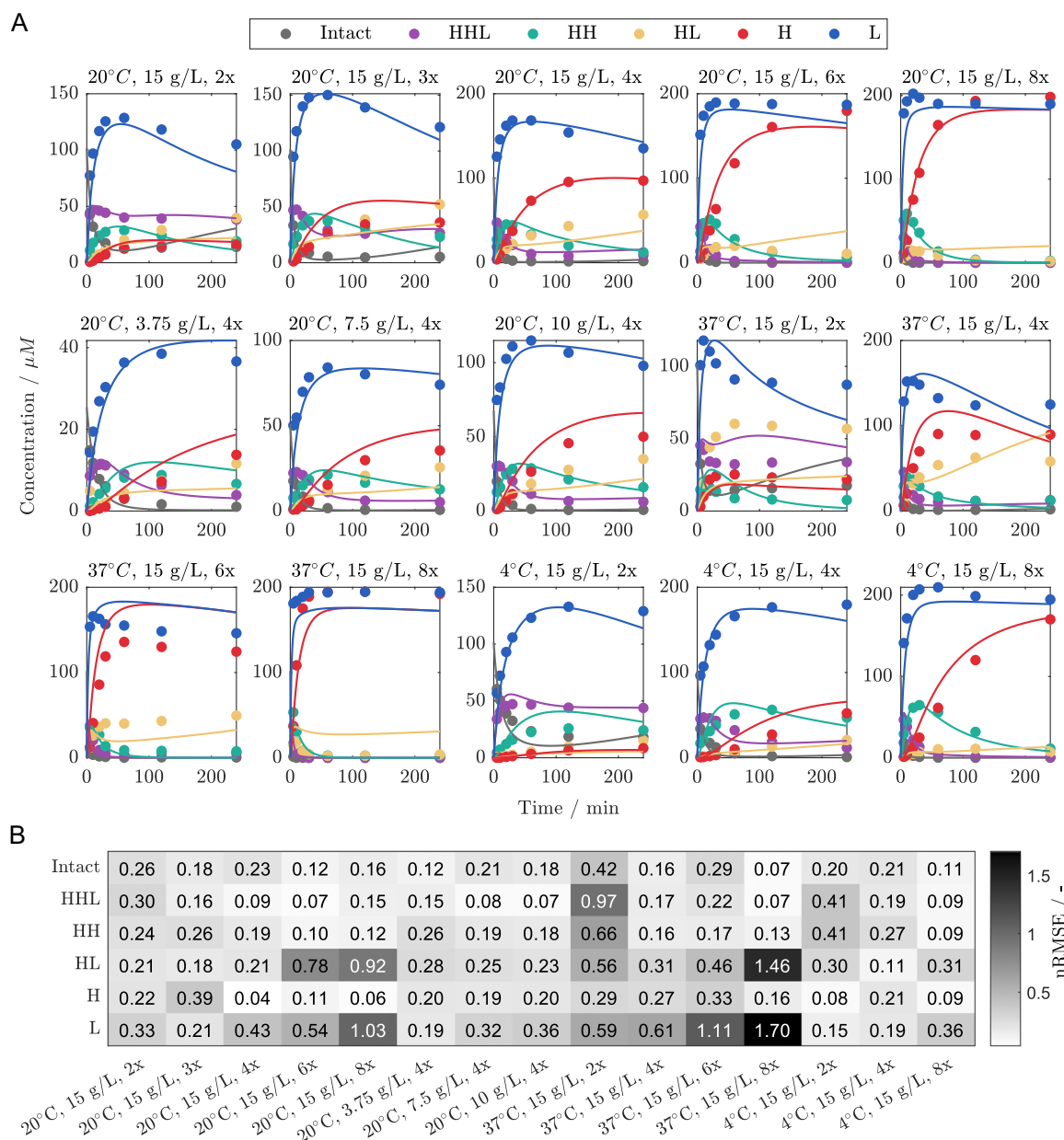


**FIGURE 4** | (A) Model predictions (lines) versus experimental CGE data (markers) for the concentrations of the six reduction species for all cross-validation runs. (B) Heatmap of the cross-validation nRMSE resolved for each individual cross-validation run in each run. Lighter colors represent a lower nRMSE value indicating smaller error, while darker colors represent higher nRMSE values or larger error.

maleimide-payloads (Kantner, Alkhawaja, and Watts 2017). Additionally, a positional switching of reduced disulfides between the inter HL and HH was recently found to occur during the moderate TCEP reduction due an intramolecular thiol-disulfide exchange (van den Berg et al. 2023). These phenomena may also contribute to the generally higher inaccuracy for the species HL and L.

### 3.2 | End-Point DAR and DLD Prediction Using MLR Models

To predict the DAR and the six DLD-% of the conjugation endpoint, MLR models were developed using either experimental CGE data or the reduction model-predicted concentrations as input. Table 3 presents the resulting  $R^2$  values for

each MLR model concerning the subsets and the model input. It has to be noted, that when using the model predictions as input, mAb2 was not further evaluated due the observed discrepancy in their reduction kinetics. With regard to the experimental values, the MLR model exhibited accurate prediction of the DAR, with  $R^2$  values close to 1 for both the training and test set. The models for DLD-% similarly achieved good performance with an average  $R^2$  of 0.973 and 0.961 for the training and test set, respectively. Generally, the prediction accuracy was highest for %H0 and %H3, while the lowest  $R^2$  value was observed for %H2, with an  $R^2$  of 0.893 for the test set. The lower performance with respect to H2 is likely to be caused by either a weaker linearity for this species or an increased analytical error due to relatively low %H2 peak levels (see Supporting Information S1: Figure S5 for an analysis of the model residuals). In total, these findings

highlight the capability of the MLR models to accurately predict the DAR/DLD-% directly from the CGE data. Support vector machine regression was initially tested as alternative, but it did not notably enhance the predictions compared to the MLR models. To the best of our knowledge, no comparable method to link CGE and RP data for ADCs has been presented in literature. A strong correlation between CGE and UHPLC was also shown for other applications (Altria and Filbey 1993; Mahan et al. 2015). Additionally, good transferability of the proposed method is shown when applying the MLR models to another mAb. Only minor losses in accuracy across all models, except H2, were observed, which is likely to be caused by slight differences in the molecule structure of the mAbs affecting the relationship between CGE and RP. Higher accuracy is expected when

training the models on data sets with a larger portion of mAb2 and/or using more advanced regression techniques that conduct an internal mAb-classification. In summary, our model approach presents a novel method to precisely forecast the RP results from CGE data with minimal practical effort.

When the MLR models were trained using the model-predicted concentrations, the accuracy is slightly reduced compared to the models using the experimental data. Still, the DAR value as well as %H0 and %H3 are precisely predicted with  $R^2$  values above 0.95. The  $R^2$  values for the other DLD-% species is slightly decreased, with %H2 exhibiting the lowest  $R^2$ . To further investigate the model's predictability uniquely for each run, the observed versus predicted plots for the DAR and the DLD-% models are shown in Figure 5. In general, these plots confirm

**TABLE 3** | Summary of  $R^2$  values for the seven MLR models using either experimental CGE data (training, test and external data (mAb2)) or reduction model-predicted data (train and test) as input. The mean DLD corresponds to the mean of the six DLD species (L0, L1, H0, H1, H2 and H3).

Input Output	Experimental CGE data			Reduction model-predicted data	
	$R^2_{\text{train}}$	$R^2_{\text{test}}$	$R^2_{\text{external}}$	$R^2_{\text{train}}$	$R^2_{\text{test}}$
DAR	0.996	0.995	0.981	0.976	0.972
%L0	0.987	0.981	0.940	0.905	0.951
%L1	0.987	0.981	0.940	0.905	0.951
%H0	0.993	0.990	0.922	0.954	0.950
%H1	0.976	0.932	0.961	0.938	0.891
%H2	0.901	0.893	0.937	0.703	0.703
%H3	0.994	0.991	0.947	0.971	0.970
Mean DLD	0.973	0.961	0.941	0.896	0.903

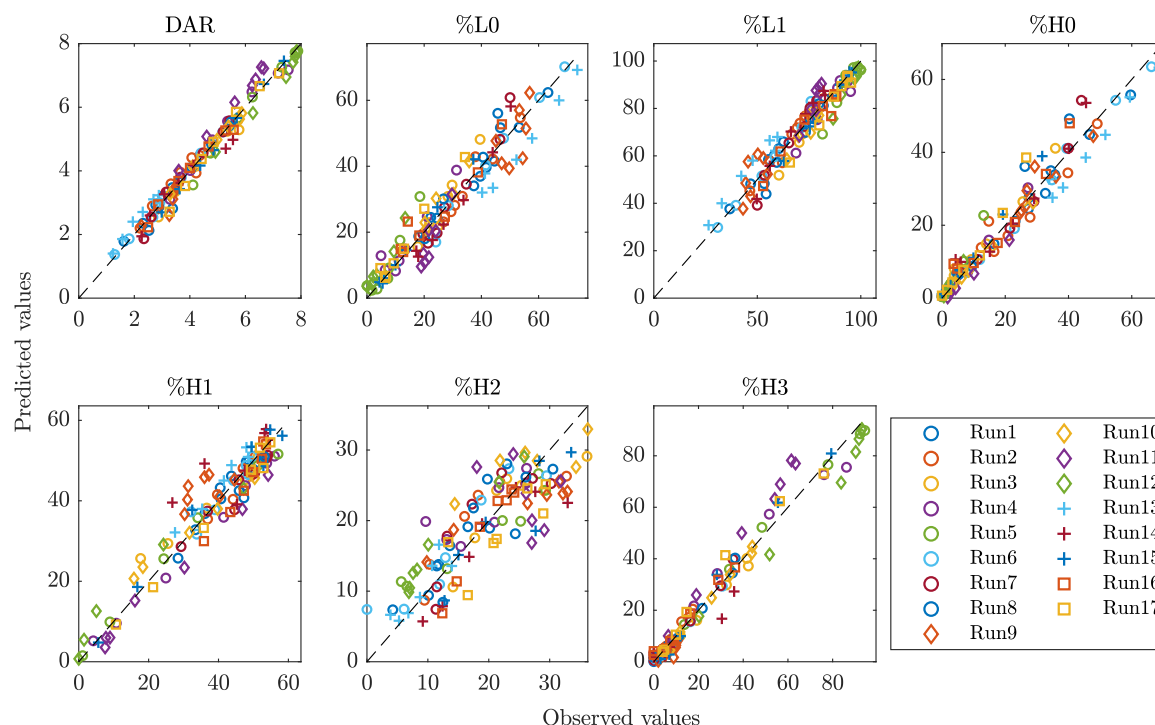


**FIGURE 5** | Observed versus predicted DAR values and DLD percentages of the MLR models using the normalized model-predicted concentrations as input. The markers are grouped according to the four temperatures (circles: 20°C, diamonds: 37°C, crosses: 4°C and squares: 12°C).

that for DAR the approach exhibits relatively higher precision compared to the DLD-%, with the lowest performance for %H2. Moreover, it becomes clear that specific runs, such as Run5, 11 and 12 contribute mainly to the larger error as indicated by their systematic offset from the regression line. This could be attributed to their larger error in the reduction kinetic model concerning certain species being propagated with the MLR model.

In total, these results highlight the capability of the MLR models to accurately predict the DAR/DLD-% also from the newly developed reduction model. For both model inputs, the models achieved better performance on the prediction of DAR compared to DLD-% which can be explained by the fact that the DAR value is calculated from all DLD-%, so that individual errors are compensated making it a more robust feature. A comparison of the model coefficients for both cases, demonstrated that the inputs species are assembled differently in the two model types (data not shown). Combined with the finding that the MLR model had to be trained independently for each instance, this suggests that the model adapts to the kinetic model error and, thus, acts as an internal model correction mechanism.

### 3.3 | Integrated In Silico Reduction Screening

Kinetic models are particularly beneficial for understanding, predicting, and evaluating the effects of reaction parameters due to

their ability to represent complex biochemical behavior. The combination of the newly developed reduction model with the different MLR models allows for the comprehensive evaluation of the effect of the reduction parameters on the resulting DAR and DLD-%, also for conditions that were not used in the model training. The resulting predictions for the DAR and two exemplary DLD-%, %L1 and %H2, based on the reduction parameter screening for the two case scenarios is provided in Figure 6 (predictions for all DLD-% and both scenarios are given in Supporting Information S1: Figures S6 and S7). For constant reaction times (Figure 6A), DAR is shown to increase with both increasing TCEP excess and temperature, reaching a plateau at the highest TCEP excess and temperature. With regard to %L1, a similar behavior compared to the DAR is observed with a slightly different influence of the temperature at lower TCEP excesses. In contrast, %H2 exhibits an inverse relationship to both parameters with a maximum around 3.5x TCEP and 37°C. The root cause for this behavior is the different temperature-dependency of the kinetic rates of inter HL and HH reduction enabling to direct conjugation to heavy or light chain. These results showcase the benefits of the proposed screening approach. While the temperature appears to have minor impact on the DAR, it seems to have a larger impact on the ratio of conjugation to light and heavy chain, especially for lower target DAR values. Knowledge of this trend is especially useful when the goal is to decrease the ratio of certain undesired species in the DLD.

Furthermore, the conjugation results for a constant temperature but for varying TCEP excess and reaction time are given in

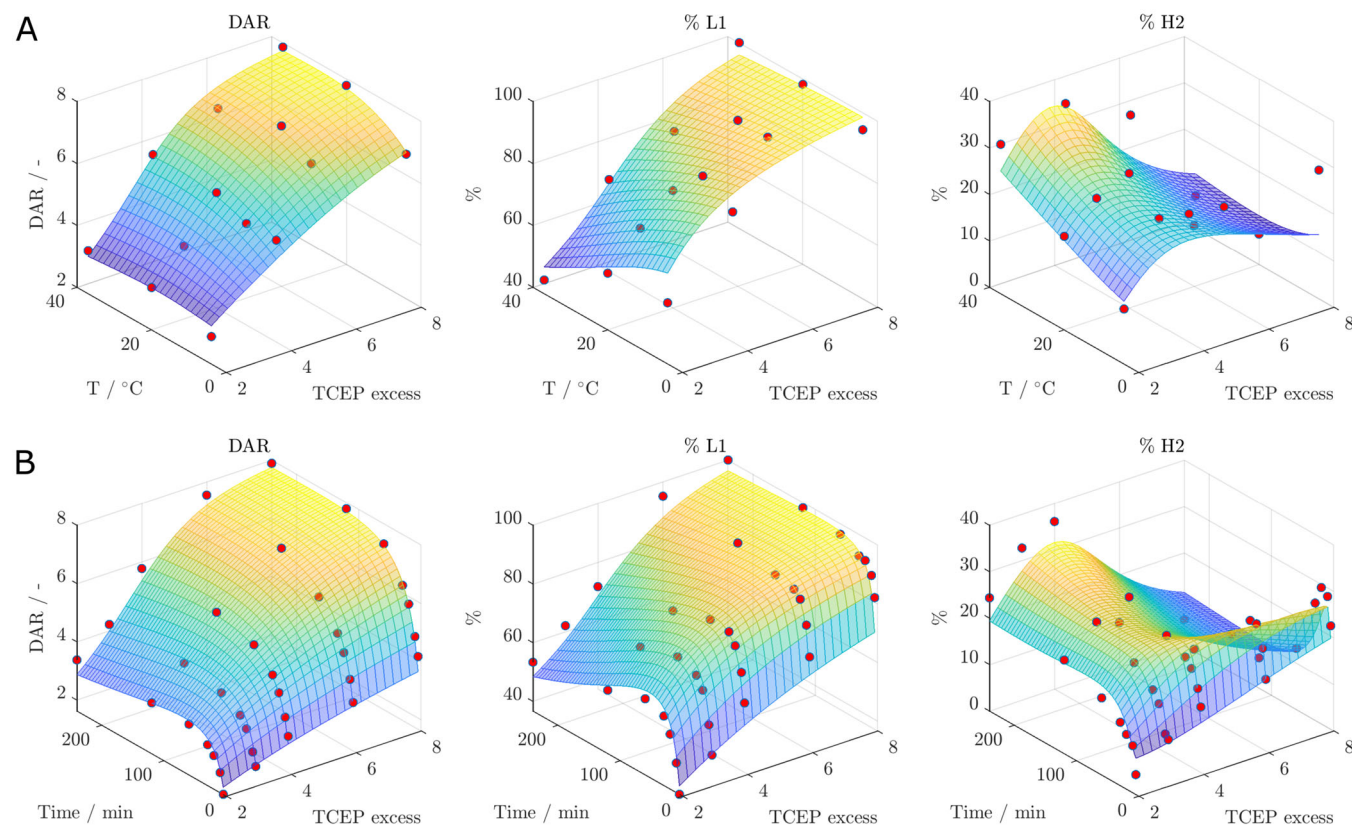


**FIGURE 6** | Integrated in silico screening for two scenarios comparing to the actual experimental data (red dots) and simulated reduction kinetics (surface plot): (A) Varying temperature and TCEP excess for constant  $c_{mAb} = 15$  g/L and  $t = 120$  min, and (B) varying reaction time and TCEP excess for constant  $c_{mAb} = 15$  g/L and  $T = 20$ °C. The surface plots represent the model predictions for DAR (left panel), %L1 (middle panel) and %H2 (right panel). Blue colors indicate lower values and yellow indicate higher values.

Figure 6B. For both DAR and %L1, the values rapidly increase for longer reaction times to a maximum and then decreases at lower TCEP excesses. This is due to the reoxidation reaction, which is particularly important for low TCEP excesses. On the contrary, %H2 has a distinct profile with a maximum at high TCEP and low reaction times, and a plateau at a TCEP excess of 4x. For longer reaction times, %H2 is only slightly affected, as the reoxidation is not occurring at the inter HH bonds. These results indicate that, in addition to the temperature and the TCEP excess, the reduction time also needs to be carefully chosen for a desired DAR value.

Overall, the *in silico* modeled surfaces capture the dynamic in the experimental data (red spheres) across the design space, with a comparably higher scattering for %H2. The comparably higher inaccuracy for %H2 might be due to the lack-of-fit of the reduction model and the lower accuracy of the MLR model for %H2. Additional experimental conditions (including replicates) following principles of Design of Experiment would need to be added, to enhance the robustness and accuracy of the model while minimizing possible bias. This would then allow for a more systematic validation of the overall screening performance. In total, these results showcase the benefit of the dual modeling approach for gaining complementary process understanding. Once this approach is validated, it can be quickly calibrated for new molecules with less kinetic data.

### 3.4 | Simulation-Based Optimization for Desired DAR

To test the model for process optimization, the model was used to find the optimal reaction time over the whole design space of temperature and TCEP excess to achieve a DAR of 3 while minimizing the %H2. Figure 7A shows the estimated reaction times as contour plot over the temperature-TCEP range. It can be seen that in the region of higher temperature and TCEP excess reaction times are short (around 5 min), while the reaction times are longer towards lower temperature and TCEP excesses. This decreasing trend in the reaction times is mainly

driven by the slower reaction rates at lower temperatures and for less reducing agent. The region for which the required level of H2 is below 12% is mainly below a temperature of approximately 12°C. To demonstrate the successful adjustment of the final DLD for the same DAR value with changing only the reduction temperature, two scenarios were considered. Figure 7B shows the predicted DLD of the two scenarios. While for condition 1, the DLD is wider containing higher levels of L0 and H2, the DLD for the improved condition 2 is narrower with lower levels of L0 and H2. This behavior results from the observed effect of the temperature on the level of H2. These two scenarios highlight that the integrated model is theoretically capable of effectively simulating alternative reaction conditions to fine-tune the DLD for the same DAR value.

## 4 | Conclusion and Outlook

This study presents the development of a reduction kinetic model for the partial reduction of the mAb interchain disulfide bonds, along with MLR modeling to directly forecast the resulting conjugation outcome at each reduction state. The data set included reduction kinetic studies under various reaction conditions, analyzed by both CGE and RP-UHPLC for quantification of the reduced species and DAR/DLD.

We first developed a reduction kinetic model by considering the CRN structure and the set of kinetic rates. Evaluating different possible CRNs revealed that the reduction reaction is driven by intermediates and reoxidation pathways, necessitating their incorporation to accurately project the reaction dynamics. Further improvements were achieved by isolating kinetic rates. This is particularly important in the sequential inter HH reduction pathway, where an acceleration of the kinetic rate for the reduction of the second inter HH bond was observed upon the reduction of the first inter HH bond, which is in accordance with recent literature findings. Adopting this method to other reducing agents would be highly interesting, as it is known that reducing agents differ in their reduction preference of certain disulfide bonds (Sun et al. 2005). Additionally, more

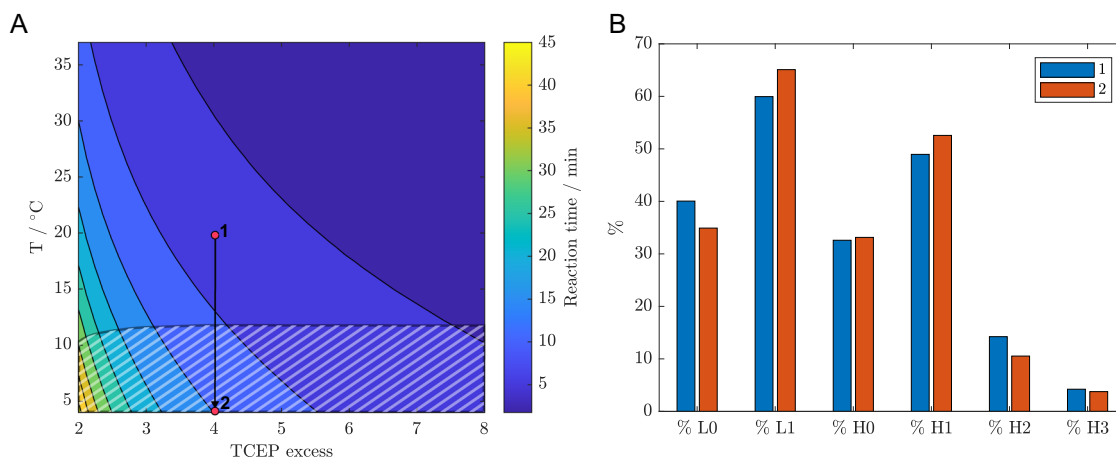


**FIGURE 7** | Contour plot of the *in silico* determined reaction times for a target DAR of 3 over the whole design space (A) and the resulting predicted DLD for two scenarios (B). The shaded area in (A) depicts the temperature-TCEP region for which the percentage of H2 is below 12%. The scenarios “1” and “2” depict two exemplary reduction conditions for the determined reaction time: Condition 1:  $T = 20^{\circ}\text{C}$  and 4x TCEP, condition 2:  $T = 4^{\circ}\text{C}$  and 4x TCEP.

sophisticated analytical approaches offering higher resolution regarding the species mass could be utilized to resolve the non-observable intermediates by CGE and validate our mechanistic findings. The temperature dependency modeled by the Arrhenius equation was unable to capture biochemical effects at higher temperatures. Further detailed experimental investigation in this temperature range or the exploration of empirical approaches to capture the temperature dependency should be considered. Comparing the reduction kinetics of different classes of mAbs for developing multi-class models would be interesting for future research.

We second established MLR-models to predict the RP-derived final DAR and DLD-% from the experimental CGE data, exhibiting remarkable performance across all outputs and the entire experimental range. Using the kinetic predictions from the newly developed kinetic model as input for the MLR models enabled direct prediction of the DAR and the DLD-% obtained after the two-step ADC reduction-conjugation workflow. However, a slight decrease in performance was attributed to the incorporation of the lack-of-fit of the reduction model, suggesting potential improvement with a more accurate reduction model.

The hereby created integrated kinetic model provided a detailed mechanistic understanding of the complex DAR/DLD-% behavior along with the reduction kinetics, as demonstrated through an in silico screening of various reduction conditions. Furthermore, this framework enabled the determination of multidimensional reaction conditions to achieve a target DAR and minimize undesired species in the DLD.

In summary, our presented methodology presents an innovative approach to capture the temperature-dependent disulfide bond reduction kinetic with a simultaneously evaluation of the possible conjugation outcome. Although the conjugation reaction conditions were set constant throughout this study, they could also be varied requiring the integration of the reduction model with a conjugation kinetic model (Weggen et al. 2024). To further enhance the utility of the reduction model, additional effects, such as pH-sensitivity of the reaction rates could be parametrized.

#### Author Contributions

**Jan Tobias Weggen:** conceptualization, methodology, data curation, formal analysis, investigation, software, visualization, writing—original draft, writing—review and editing. **Pedro González:** methodology, software, visualization. **Kimberly Hui:** investigation, data curation, formal analysis, writing—review and editing. **Ryan Bean:** investigation, data curation, formal analysis. **Michaela Wendeler:** conceptualization, supervision, project administration, funding acquisition, writing—review and editing. **Jürgen Hubbuch:** conceptualization, supervision, funding acquisition, writing—review and editing.

#### Acknowledgments

The authors would like to thank Annabelle Dietrich and Robin Schiemer for careful proof-reading of the manuscript. We also would like to thank William Keller for his valuable input. Open Access funding enabled and organized by Projekt DEAL.

#### Conflicts of Interest

Authors Michaela Wendeler, Ryan Bean and Kimberly Hui are employed by AstraZeneca and report stock ownership and/or stock options or interest in AstraZeneca. The authors declare that the research was conducted in the absence of any commercial or financial relationships that could be construed as a potential conflict of interest.

#### Data Availability Statement

The data that support the findings of this study are available from the corresponding author upon reasonable request.

#### References

- Adem, Y. T., K. A. Schwarz, E. Duenas, T. W. Patapoff, W. J. Galush, and O. Esue. 2014. “Auristatin Antibody Drug Conjugate Physical Instability and the Role of Drug Payload.” *Bioconjugate Chemistry* 25, no. 4: 656–664. <https://doi.org/10.1021/bc400439x>.
- Altria, K. D., and S. D. Filbey. 1993. “Quantitative Pharmaceutical Analysis by Capillary Electrophoresis.” *Journal of Liquid Chromatography* 16, no. 11: 2281–2292. <https://doi.org/10.1080/10826079308020985>.
- Andris, S., J. Seidel, and J. Hubbuch. 2019. “Kinetic Reaction Modeling for Antibody-Drug Conjugate Process Development.” *Journal of Biotechnology* 306, no. September: 71–80. <https://doi.org/10.1016/j.jbiotec.2019.09.013>.
- Behrens, C. R., E. H. Ha, L. L. Chinn, et al. 2015. “Antibody-Drug Conjugates (ADCs) Derived From Interchain Cysteine Cross-Linking Demonstrate Improved Homogeneity and Other Pharmacological Properties Over Conventional Heterogeneous ADCs.” *Molecular Pharmaceutics* 12, no. 11: 3986–3998. <https://doi.org/10.1021/acs.molpharmaceut.5b00432>.
- Behrens, C. R., and B. Liu. 2014. “Methods for Site-Specific Drug Conjugation to Antibodies.” *mAbs* 6, no. 1: 46–53. <https://doi.org/10.4161/mabs.26632>.
- van den Berg, E. B. A., J. C. W. Hendriks, E. W. Elsinga, M. Eggink, and E. H. C. Dirksen. 2023. “Switching Positions: Assessing the Dynamics of Conjugational Heterogeneity in Antibody-Drug Conjugates Using CE-SDS.” *Electrophoresis* 44, no. 1–2: 62–71. <https://doi.org/10.1002/elps.202200140>.
- Cao, M., N. De Mel, Y. Jiao, et al. 2019. “Site-Specific Antibody-Drug Conjugate Heterogeneity Characterization and Heterogeneity Root Cause Analysis.” *mAbs* 11, no. 6: 1064–1076. <https://doi.org/10.1080/19420862.2019.1624127>.
- Chau, C. H., P. S. Steeg, and W. D. Figg. 2019. “Antibody-Drug Conjugates for Cancer.” *Lancet* 394, no. 10200: 793–804. [https://doi.org/10.1016/S0140-6736\(19\)31774-X](https://doi.org/10.1016/S0140-6736(19)31774-X).
- Chen, H., D. Qiu, J. Shi, et al. 2024. “In-Depth Structure and Function Characterization of Heterogeneous Interchain Cysteine-Conjugated Antibody – Drug Conjugates.” *ACS Pharmacology & Translational Science* 7: 212–221. <https://doi.org/10.1021/acspstsci.3c00235>.
- Chen, T., D. Su, J. Gruenhagen, et al. 2016. “Chemical De-Conjugation for Investigating the Stability of Small Molecule Drugs in Antibody-Drug Conjugates.” *Journal of Pharmaceutical and Biomedical Analysis* 117: 304–310. <https://doi.org/10.1016/j.jpba.2015.09.015>.
- Chou, I. C., and E. O. Voit. 2009. “Recent Developments in Parameter Estimation and Structure Identification of Biochemical and Genomic Systems.” *Mathematical Biosciences* 219, no. 2: 57–83. <https://doi.org/10.1016/j.mbs.2009.03.002>.
- Forster, T., D. Vázquez, M. N. Cruz-Bournazou, A. Butté, and G. Guillén-Gosálbez. 2023. “Modeling of Bioprocesses Via Minlp-Based Symbolic Regression of S-System Formalisms.” *Computers & Chemical Engineering* 170, no. December 2022: 108108. <https://doi.org/10.1016/j.compchemeng.2022.108108>.

- Fromer, J., C. Georgakis, and J. Mustakis. 2023. "Toward the Identification of Stoichiometric Models for Complex Reaction Mixtures." *Industrial & Engineering Chemistry Research* 62, no. 5: 2225–2239. <https://doi.org/10.1021/acs.iecr.2c01231>.
- Fu, Z., S. Li, S. Han, C. Shi, and Y. Zhang. 2022. "Antibody Drug Conjugate: The "Biological Missile" for Targeted Cancer Therapy." *Signal Transduction and Targeted Therapy* 7, no. 1: 93. <https://doi.org/10.1038/s41392-022-00947-7>.
- Gordon, M. R., M. Canakci, L. Li, J. Zhuang, B. Osborne, and S. Thayumanavan. 2015. "Field Guide to Challenges and Opportunities in Antibody-Drug Conjugates for Chemists." *Bioconjugate Chemistry* 26, no. 11: 2198–2215. <https://doi.org/10.1021/acs.bioconjchem.5b00399>.
- Guo, J., S. Kumar, M. Chipley, et al. 2016. "Characterization and Higher-Order Structure Assessment of an Interchain Cysteine-Based ADC: Impact of Drug Loading and Distribution on the Mechanism of Aggregation." *Bioconjugate Chemistry* 27, no. 3: 604–615. <https://doi.org/10.1021/acs.bioconjchem.5b00603>.
- Hutterer, K. M., R. W. Hong, J. Lull, et al. 2013. "Monoclonal Antibody Disulfide Reduction During Manufacturing Untangling Process Effects From Product Effects." *mAbs* 5, no. 4: 608–613. <https://doi.org/10.4161/mabs.24725>.
- ICH 2008. Q8 (R2) Pharmaceutical Development. ICH Q9 (Quality Risk Management). ICH Q 10.
- Ji, W., and S. Deng. 2021. "Autonomous Discovery of Unknown Reaction Pathways From Data by Chemical Reaction Neural Network." *Journal of Physical Chemistry A* 125, no. 4: 1082–1092. <https://doi.org/10.1021/acs.jpca.0c09316>.
- Kamath, A. V., and S. Iyer. 2015. "Preclinical Pharmacokinetic Considerations for the Development of Antibody Drug Conjugates." *Pharmaceutical Research* 32, no. 11: 3470–3479. <https://doi.org/10.1007/s11095-014-1584-z>.
- Kantner, T., B. Alkhwaja, and A. G. Watts. 2017. "In Situ Quenching of Trialkylphosphine Reducing Agents Using Water-Soluble PEG-Azides Improves Maleimide Conjugation to Proteins." *ACS Omega* 2, no. 9: 5785–5791. <https://doi.org/10.1021/acsomega.7b01094>.
- Khongorzul, P., C. J. Ling, F. U. Khan, A. U. Ihsan, and J. Zhang. 2020. "Antibody-Drug Conjugates: A Comprehensive Review." *Molecular Cancer Research* 18, no. 1: 3–19. <https://doi.org/10.1158/1541-7786.MCR-19-0582>.
- Liu, H., C. Chumsae, G. Gaza-Bulsecu, K. Hurkmans, and C. H. Radziejewski. 2010. "Ranking the Susceptibility of Disulfide Bonds in Human IgG1 Antibodies by Reduction, Differential Alkylation, and LC-MS Analysis." *Analytical Chemistry* 82, no. 12: 5219–5226. <https://doi.org/10.1021/ac100575n>.
- Mahan, A. E., J. Tedesco, K. Dionne, et al. 2015. "A Method for High-Throughput, Sensitive Analysis of IgG Fc and Fab Glycosylation by Capillary Electrophoresis." *Journal of Immunological Methods* 417: 34–44. <https://doi.org/10.1016/j.jim.2014.12.004>.
- Matsuda, Y., and B. A. Mendelsohn. 2021. "An Overview of Process Development for Antibody-Drug Conjugates Produced by Chemical Conjugation Technology." *Expert Opinion on Biological Therapy* 21, no. 7: 963–975. <https://doi.org/10.1080/14712598.2021.1846714>.
- Matsuda, Y., Z. Tawfiq, M. Leung, and B. A. Mendelsohn. 2020. "Insight Into Temperature Dependency and Design of Experiments Towards Process Development for Cysteine-Based Antibody-Drug Conjugates." *ChemistrySelect* 5, no. 28: 8435–8439. <https://doi.org/10.1002/slct.202001822>.
- Metrangolo, V., and L. H. Engelholm. 2024. "Antibody-Drug Conjugates: The Dynamic Evolution From Conventional to Next-Generation Constructs." *Cancers* 16, no. 2: 447. <https://doi.org/10.3390/cancers16020447>.
- Nadkarni, D. V., Q. Jiang, O. Friese, et al. 2018. "Process Development and Structural Characterization of an Anti-Notch 3 Antibody-Drug Conjugate." *Organic Process Research & Development* 22, no. 3: 286–295. <https://doi.org/10.1021/acs.oprd.7b00337>.
- Narayanan, H., M. F. Luna, M. von Stosch, et al. 2020. "Bioprocessing in the Digital Age: The Role of Process Models." *Biotechnology Journal* 15, no. 1: 1–10. <https://doi.org/10.1002/biot.201900172>.
- Nayak, S., and S. M. Richter. 2023. "Kinetic Studies of the Partial Reduction and Conjugation Reactions in an Antibody-Drug Conjugate (ADC) Synthesis." *Organic Process Research & Development* 27: 2091–2099. <https://doi.org/10.1021/acs.oprd.3c00264>.
- Prashad, A. S., B. Nolting, V. Patel, A. Xu, B. Arve, and L. Letendre. 2017. "From R&D to Clinical Supplies." *Organic Process Research and Development* 21, no. 4: 590–600. <https://doi.org/10.1021/acs.oprd.7b00020>.
- Sänger-van de Griend, C. E. 2019. "CE-SDS Method Development, Validation, and Best Practice—An Overview." *Electrophoresis* 40, no. 18–19: 2361–2374. <https://doi.org/10.1002/elps.201900094>.
- Sasso, J. M., R. Tenchov, R. Bird, et al. 2023. "The Evolving Landscape of Antibody-Drug Conjugates: In Depth Analysis of Recent Research Progress." *Bioconjugate Chemistry* 34, no. 11: 1951–2000. <https://doi.org/10.1021/acs.bioconjchem.3c00374>.
- Schwaab, M., and J. C. Pinto. 2007. "Optimum Reference Temperature for Reparameterization of the Arrhenius Equation. Part 1: Problems Involving One Kinetic Constant." *Chemical Engineering Science* 62, no. 10: 2750–2764. <https://doi.org/10.1016/j.ces.2007.02.020>.
- Sin, G., and K. Gernaey. 2016. "Data Handling and Parameter Estimation." In *Experimental Methods in Wastewater Treatment*, edited by M. C. M. van Loosdrecht, P. H. Nielsen, C. M. Lopez-Vazquez, and D. Brdjanovic, 201–234. IWA Publishing.
- Smiatek, J., A. Jung, and E. Bluhmki. 2020. "Towards a Digital Bioprocess Replica: Computational Approaches in Biopharmaceutical Development and Manufacturing." *Trends in Biotechnology* 38, no. 10: 1141–1153. <https://doi.org/10.1016/j.tibtech.2020.05.008>.
- Song, Y., H. Cai, Z. Tan, N. Mussa, and Z. J. Li. 2022. "Mechanistic Insights Into Inter-Chain Disulfide Bond Reduction of IgG1 and IgG4 Antibodies." *Applied Microbiology and Biotechnology* 106, no. 3: 1057–1066. <https://doi.org/10.1007/s00253-022-11778-5>.
- Sun, M. M. C., K. S. Beam, C. G. Cervený, et al. 2005. "Reduction-Alkylation Strategies for the Modification of Specific Monoclonal Antibody Disulfides." *Bioconjugate Chemistry* 16, no. 5: 1282–1290. <https://doi.org/10.1021/bc050201y>.
- Tang, P., Z. Tan, V. Ehamparanathan, et al. 2020. "Optimization and Kinetic Modeling of Interchain Disulfide Bond Reoxidation of Monoclonal Antibodies in Bioprocesses." *mAbs* 12, no. 1. <https://doi.org/10.1080/19420862.2020.1829336>.
- Taylor, C. J., A. Pomberger, K. C. Felton, et al. 2023. "A Brief Introduction to Chemical Reaction Optimization." *Chemical Reviews* 123: 3089–3126. <https://doi.org/10.1021/acs.chemrev.2c00798>.
- Taylor, C. J., H. Seki, F. M. Dannheim, et al. 2021. "An Automated Computational Approach to Kinetic Model Discrimination and Parameter Estimation." *Reaction Chemistry & Engineering* 6, no. 8: 1404–1411. <https://doi.org/10.1039/d1re00098e>.
- Wang, T., Y. D. Liu, B. Cai, G. Huang, and G. C. Flynn. 2015. "Investigation of Antibody Disulfide Reduction and Re-Oxidation and Impact to Biological Activities." *Journal of Pharmaceutical and Biomedical Analysis* 102: 519–528. <https://doi.org/10.1016/j.jpba.2014.10.023>.
- Weggen, J. T., R. Bean, K. Hui, M. Wendeler, and J. Hubbuch. 2024. "Kinetic Models Towards an Enhanced Understanding of Diverse ADC Conjugation Reactions." *Frontiers in Bioengineering and Biotechnology* 12: 1403644. <https://doi.org/10.3389/fbioe.2024.1403644>.

You, J., J. Zhang, J. Wang, and M. Jin. 2021. "Cysteine-Based Coupling: Challenges and Solutions." *Bioconjugate Chemistry* 32, no. 8: 1525–1534. <https://doi.org/10.1021/acs.bioconjchem.1c00213>.

### Supporting Information

Additional supporting information can be found online in the Supporting Information section.